Chapter 19

RAMAN SPECTROSCOPY OF GRAPHENE AND RELATED MATERIALS

Isaac Childres*[a,b], Luis A. Jauregui[b,c], Wonjun Park[b,c], Helin Cao[a,b] and Yong P. Chen[a,b,c]

[a]Department of Physics, Purdue University, West Lafayette, IN, US
[b]Birck Nanotechnology Center, Purdue University, West Lafayette, IN, US
[c]School of Electrical and Computer Engineering, Purdue University, West Lafayette, IN, US

ABSTRACT

This chapter is a review of the application of Raman spectroscopy in characterizing the properties of graphene, both exfoliated and synthesized, and graphene-based materials such as graphene-oxide. Graphene is a 2-dimensional honeycomb lattice of sp2-bonded carbon atoms and has received enormous interest because of its host of interesting material properties and technological potentials. Raman spectroscopy (and Raman imaging) has become a powerful, noninvasive method to characterize graphene and related materials. A large amount of information such as disorder, edge and grain boundaries, thickness, doping, strain and thermal conductivity of graphene can be learned from the Raman spectrum and its behavior under varying physical conditions. In particular, this chapter will discuss Raman characterization of graphene with artificial disorder generated by irradiations

* E-mail address: ichildre@purdue.edu

such as electron-beam exposure and oxygen plasma, focusing on the defect-activated Raman D peak.

1. INTRODUCTION

Graphene is a 2-dimensional (2-D) hexagonal lattice of carbon atoms [Fig. 1(a)]. Its 2-D nature leads to a linear dispersion relation at the K points of the Brilluion zone [Fig. 1(b)], also known as a "Dirac" cone, and this linear dispersion necessarily implies that charge carriers in the graphene have no rest mass, leading to a host of interesting electronic properties including high room-temperature mobility [1].

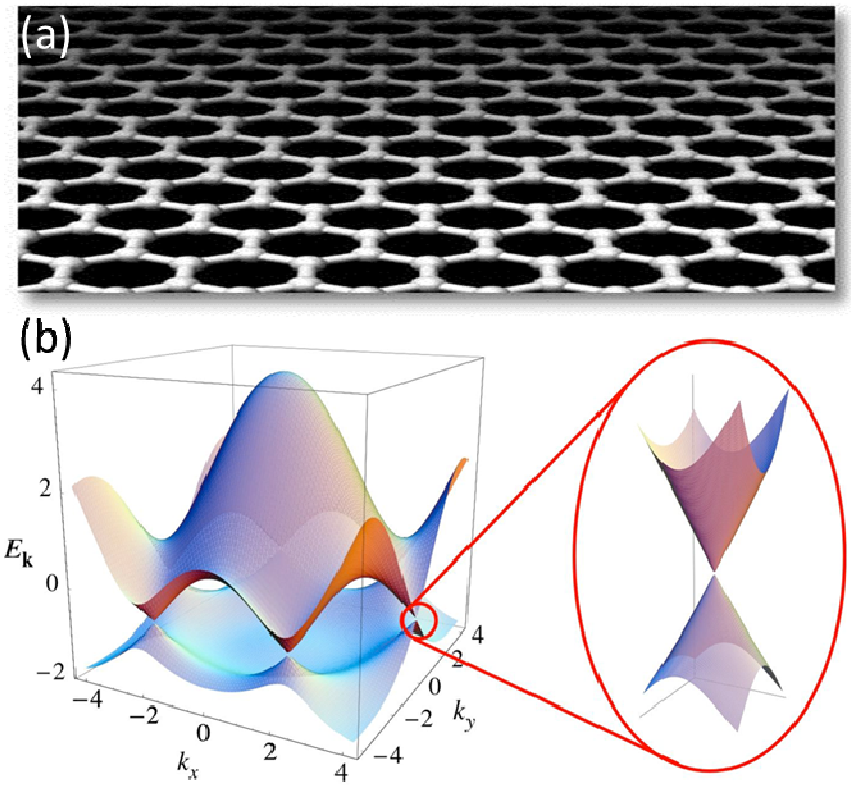

Figure 1. (Color online) (a) Carbon hexagonal lattice structure of graphene. (b) Graphene is a zero-gap semiconductor. Its 2-D nature leads to a linear dispersion relation at the unequivalent K and K´ points of the Brilluion zone, also known as a "Dirac" cone.

Graphene has received much attention recently in the scientific community because of its distinct properties and potentials in nanoelectronic applications [2]. Many reports have been made not only on graphene's very high electrical conductivity at room temperature [1, 3] but also its potential use as next-generation transistors [4], nano-sensors [5], transparent electrodes [6] and many other applications.

In this review, we will focus on the application of Raman spectroscopy in characterizing the properties of graphene, both exfoliated and synthesized, and graphene-based materials such as graphene-oxide. Raman spectroscopy uses a monochromatic laser to interact with molecular vibrational modes and phonons in a sample, shifting the laser energy down (Stokes) or up (anti-Stokes) through inelastic scattering [7]. Identifying vibrational modes using only laser excitation, Raman spectroscopy has become a powerful, noninvasive method to characterize graphene and related materials [8]. We will discuss how characteristics such as disorder, edge and grain boundaries, thickness, doping, strain and thermal conductivity of graphene can be learned from Raman spectroscopy.

2. RAMAN SPECTROSCOPY OF GRAPHENE

In graphene, the Stokes phonon energy shift caused by laser excitation creates two main peaks in the Raman spectrum: G (1580 cm^{-1}), a primary in-plane vibrational mode, and 2D (2690 cm^{-1}), a second-order overtone of a different in-plane vibration, D (1350 cm^{-1}) [8]. D and 2D peak positions are dispersive (dependent on the laser excitation energy) [9]. The positions cited are from a 532 nm excitation laser.

Because of added forces from the interactions between layers of AB-stacked graphene, as the number of graphene layers increases, the spectrum will change from that of single-layer graphene, namely a splitting of the 2D peak into an increasing number of modes that can combine to give a wider, shorter, higher frequency peak [10]. The G peak also experiences a smaller red shift from increased number of layers [11]. Thus, for AB-stacked graphene, the number of layers can be derived from the ratio of peak intensities, I_{2D}/I_G, as well as the position and shape of these peaks [10]. Rotationally disordered (decoupled) multilayer graphene, however, can still have a single intense 2D peak regardless of thickness [12], though its position and FWHM can depend on the number of layers [10, 13]. A comparison of the Raman spectra of single-layer graphene and bulk graphite (A-B stacked) can be seen in Fig. 2(a).

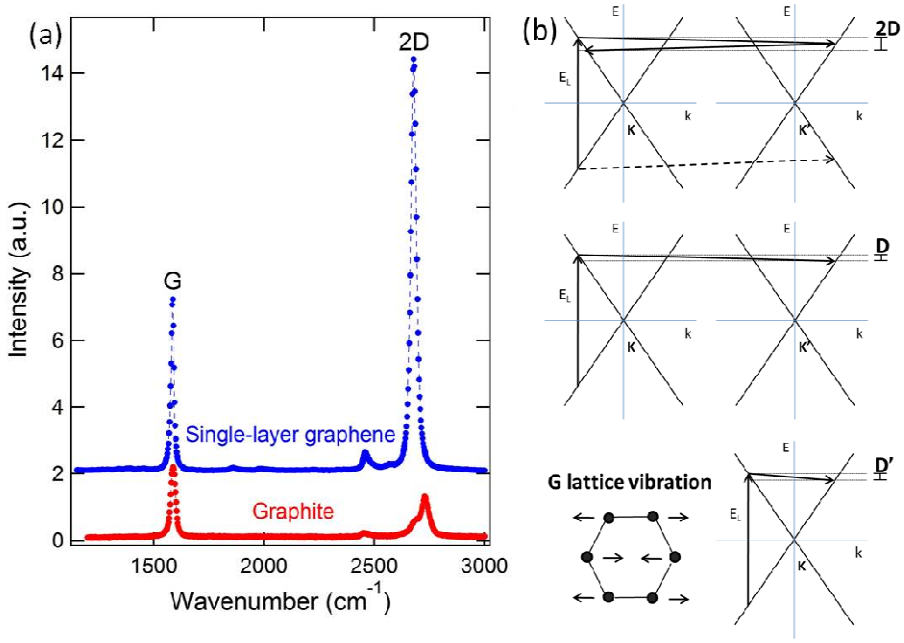

Figure 2. (Color online) (a) Typical Raman spectra for a single-layer graphene sample and bulk graphite using a 532 nm excitation laser. The spectra are offset vertically for clarity. Graphene can be identified by the position and shape of its G (1580 cm^{-1}) and 2D (2690 cm^{-1}) peaks. (b) Graphical representations of examples of phonon scattering processes responsible for the significant graphene Raman peaks. The D (intervalley phonon and defect scattering) and D´ (intravalley phonon and defect scattering) peaks appear in disordered graphene. The 2D peak involves double phonon scattering (either both on a single electron/hole or on an electron-hole pair [16, 17]).

The first-order D peak itself is not visible in pristine graphene because of crystal symmetries [14]. In order for a D peak to occur, a charge carrier must be excited and inelastically scattered by a phonon, then a second elastic scattering by a defect or zone boundary must occur to result in recombination [15]. The second-order overtone, 2D, is always allowed because the second scattering (either on the initially scattered electron/hole or its complementary hole/electron) in the process is also an inelastic scattering from a second phonon [see Fig. 2(b)] [16, 17].

As the amount of disorder in graphene increases, the Raman intensity increases for the three separate disorder peaks: D (1350 cm^{-1}), which scatters from K to K´ (intervalley); D´ (1620 cm^{-1}), which scatters from K to K (intravalley); and D+G (2940 cm^{-1}), a combination scattering peak [8, 18]. These peaks can be

seen in Fig. 3(a), with an illustration of the electron-phonon scattering mechanism for all major peaks seen in Fig. 2(b).

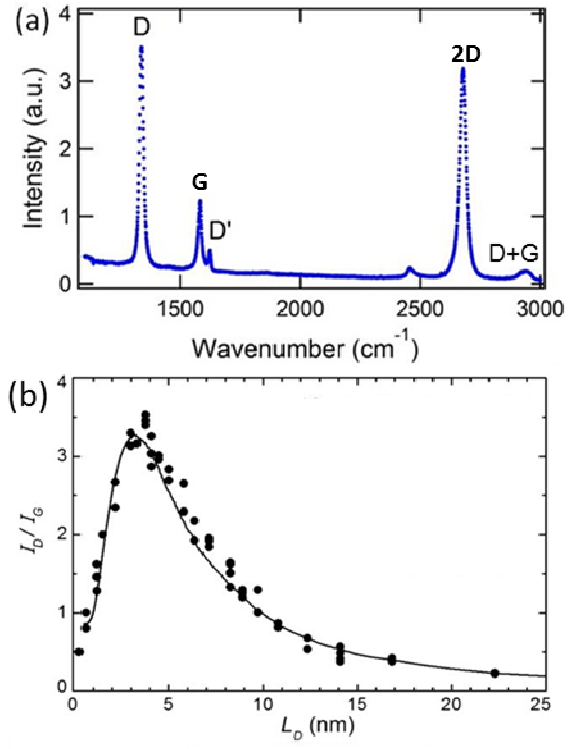

Figure 3. (Color online) (a) Raman spectrum of graphene irradiated by electron beam, showing significant D, D´ and D+G disorder peaks. The concentration of disorder can be extracted from the intensity ratio I_D/I_G. I_D/I_G ~ 3 for this spectrum. (b) (From [19]) I_D/I_G directly related to the average distance between defects (L_D) measured by STM, showing a well-behaved trend.

Using the ratio of peak intensities I_D/I_G, one can use Raman spectra to characterize the level of disorder in graphene. As disorder in graphene increases, I_D/I_G displays 2 different behaviors. There is a regime of "low" defect density where I_D/I_G will increase as a higher defect density creates more elastic scattering. This occurs up to a regime of "high" defect density, at which point I_D/I_G will begin to decrease as an increasing defect density results in a more amorphous carbon structure, attenuating all Raman peaks [19]. These two regimes are

referred to as "nanocrystalline graphite" and "mainly sp^2 amorphous carbon" phases, respectively [8, 19-23].

These two separate regimes are caused by two separate areas of influence around specific defect sites: an area within a radius, r_s, which has structural disorder and enhances the D peak weakly; and an area within a larger radius, r_a, which is still close enough to the defect site to be activated, enhancing the D peak strongly [19]. Graphene is considered to be in the nanocrystalline graphite regime for the average distance between defects, $L_D > 2r_a$. Reference [19] proposes using the following equation to describe the enhancement of the D peak in both regimes, relating L_D to the ratio of Raman peak intensities, I_D/I_G:

$$\frac{I_D}{I_G} = C_a \frac{r_a^2 - r_s^2}{r_a^2 - 2r_s^2}\left[\exp(-\frac{\pi r_s^2}{L_D^2}) - \exp(-\frac{\pi(r_a^2 - r_s^2)}{L_D^2})\right] + C_a\left[1 - xp(-\frac{\pi r_s^2}{L_D^2})\right] \quad (1)$$

Here C_a and C_s are parameters describing the strength of the influence the corresponding region has on the intensity of the D peak. It is possible that C_a and C_s may be dependent on the type of defect created, whether it is a dopant atom or a structural anomaly. This fitting can be seen in Fig. 3(b). Note that Eq. (1) may not hold for when L_D becomes so small for some types of disorder that cause a breakdown of the graphene lattice (and no more discernible Raman D-peak).

It has also been proposed that the relation between I_D/I_G and L_D can be approximated by two empirical formulas for the two separate regimes. In the low-defect-density regime [19]:

$$\frac{I_D}{I_G} = \frac{C(\lambda)}{L_D^2}, \quad (2)$$

where λ is the Raman excitation wavelength and $C(\lambda) = 102$ nm^2 for $\lambda = 514$ nm [19]. This equation is different from the Tuinstra-Koenig relation [14]

$$\frac{I_D}{I_G} = \frac{C'(\lambda)}{L_D}, \quad (3)$$

where $C'(\lambda) = (2.4 \cdot 10^{-10}\ \text{nm}^{-3}) \cdot \lambda^4$ [24]. Equation (3) is valid for edge defects rather than point defects [19].

In the high-defect-density regime, approaching a full breakdown of the carbon lattice, I_D/I_G versus L_D has been fitted to the equation [8, 23, 24]

$$\frac{I_D}{I_G} = D(\lambda) \times L_D^2 \tag{4}$$

where the constant $D(\lambda)$ is obtained by imposing continuity between the two regimes.

3. GRAPHENE-BASED MATERIALS

Graphene can be fabricated using a variety of methods. In our experimental work, two main methods are used: exfoliation and chemical vapor deposition (CVD). A common method for graphene exfoliation is the Scotch tape method [1], where thin sheets of graphite are peeled from a bulk graphite sample using adhesive tape, then thinned further with subsequent tape-to-tape peelings. Eventually the graphene is ready to peel onto the SiO_2/Si substrate when it becomes semi-transparent and dispersed onto the tape in many smaller crystals, some of which are single-layer.

This peeling process works because the carbon layers of graphite are weakly bonded and the van der Waals force between them is not as strong as the force between the graphite/graphene and the SiO_2. So, once the graphite pieces on the tape are applied to the substrate, it is likely that when the tape is lifted the interlayer bonds will break, leaving some amount of graphite/graphene on the substrate [25]. Newly peeled single-layer graphene will show prominent G and 2D peaks in its Raman spectra.

CVD synthesized graphene is made by depositing or segregating carbon decomposed from precursor gases containing hydrocarbons such as CH_4 onto metal catalyst foils (commonly Ni or Cu) at high temperatures, followed by a cool down [26-31].

Early films grown on Ni with this technique resulted in slightly disordered graphene films of non-uniform thickness, as characterized by Raman spectroscopy [29]. Figure 4(a) [29] shows Raman spectra from various spots of a CVD graphene film grown on Ni. Each spectra is different because of varying layer thickness (size, shape and position of 2D peak) and disorder (size of D peak). Currently Cu is widely regarded as a superior metal on which to grow CVD graphene films [30, 31]. Figure 4(b) [31] shows Raman spectra from various spots of a film grown on Cu. The spectra are more uniform, showing a low-disorder single-layer film.

Another method of creating graphene-like materials is through the exfoliation and reduction of graphene oxide [32]. Graphene oxide is produced through an oxygen-producing chemical reaction within the layers of a graphite crystal. This graphene oxide is then exfoliated in situ via sonication and then reduced with hydrazine hydrate, producing a material with some electrical properties approximating graphene. Raman spectra of the materials, as seen in Fig. 5 [33], show strong D and G peaks, suggesting very small crystal sizes.

Graphitic composite materials can also be made by adding polymers to the reduced graphene oxide in solution. These materials retain some of the electrical properties of graphene while also retaining the physical properties of a polymer [32, 34].

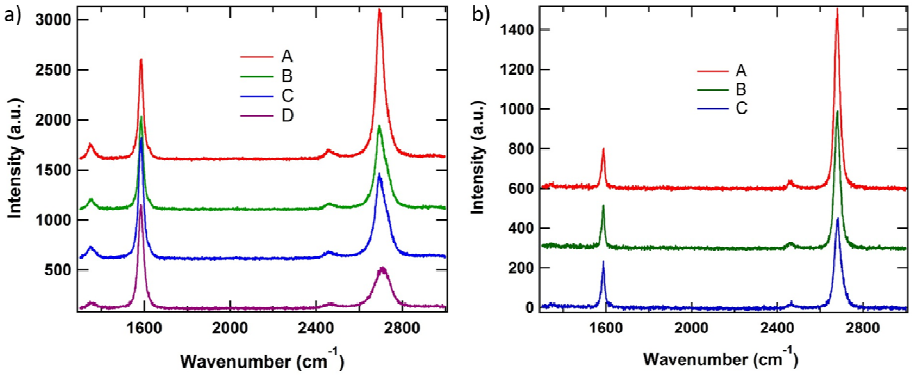

Figure 4. (Color online) (a) (From [29]) Representative Raman spectra (excitation wavelength 532 nm) measured from 4 spots on a CVD graphene film grown on a Ni substrate and transferred to SiO_2/Si. (b) (From [31]) Representative Raman spectra measured from 3 spots on a CVD graphene film grown on a Cu substrate and transferred to SiO_2/Si.

4. Characterization of Graphene Properties Through Raman Sepctroscopy

In addition to characterizing disorder and L_D, Raman spectroscopy can also be used to characterize many other properties in graphene, including the edges and grain boundaries of graphene crystals [35-39]. Due to the hexagonal structure of the graphene lattice, ordered crystal edges can have two main structures: zigzag and armchair (Fig. 6 [39]). Only armchair edges, however, are capable of elastically scattering charge carriers that give rise to the D peak [37, 39].

Reference [39] showed that a strong D peak will appear near armchair edges using an excitation laser polarized in a direction parallel to the line of the edge. This effect is significantly smaller for zigzag edges, where some amount of D intensity is still seen in real samples because of non-uniformity and roughness in edge structure.

In has also been theorized and supported by experiment that only the longitudinal optical phonon mode is active near an armchair edge, and the transverse optical phonon mode is active near a zigzag edge, so that the intensity of the G peak is enhanced when the polarization of the excitation laser is parallel to an armchair edge and perpendicular to a zigzag edge [40-42].

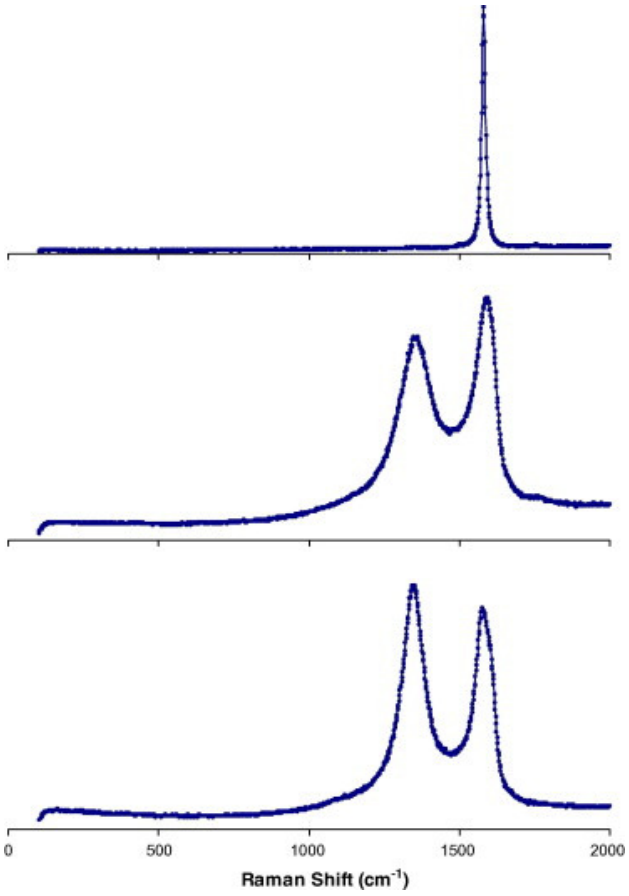

Figure 5. (Color online) (From [33]) The Raman spectra of SP-1 grade graphite (top), graphene oxide (middle), and reduced graphene oxide (bottom).

Characterization of edges is not only useful in differentiating between zigzag and armchair, but also in characterizing the grain boundaries of CVD graphene crystals. Where grains from two separate seed points grow together, a boundary forms that is identifiable through an increased D peak, providing insight into the crystal growth process. The nucleation center of these crystals is also characterized by a higher D peak [43].

Doping in graphene, which shifts the Fermi level away from the Dirac point, decreases the probability of excited charge carrier recombination [44]. This causes photon perturbations to be non-adiabatic, removing the Kohn anomaly and increasing the phonon energy for the G peak, increasing its frequency [45]. This reduced recombination also sharpens the G peak, decreasing its FWHM. Das *et al* also theorize increased electron concentration (decreased hole concentration) expands the crystal lattice, decreasing the energy of the Raman phonons, resulting in a decreased 2D peak position with increased electron concentration and an asymmetry in the doping effect of the G peak position. Doping graphene also decreases the intensity of the 2D peak.

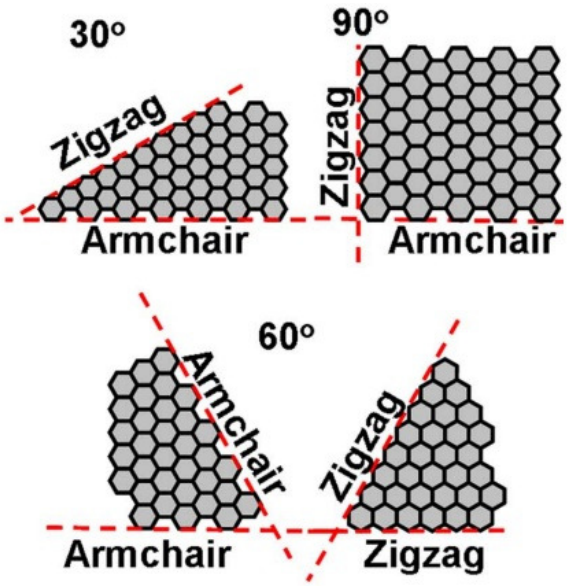

Figure 6. (Color online) (From [39]) Illustration of the relationship between corner angles and the structure of adjacent graphene edges.

In addition to doping, this expansion and contraction of the crystal lattice can also be achieved through physical strain on the graphene, often caused by a lattice mismatch with the underlying substrate [46-51]. As with doping effects, a

stretching of the lattice would decrease the phonon energies, causing a red shift of the Raman spectrum. If this strain is uniaxial, as in the case of bending, it will also split the G peak into two separate features corresponding to the splitting of the vibrational mode into one along an axis parallel to the curvature and one perpendicular.

These varied effects give many tools to characterize the electron concentration and lattice strain in a graphene sample.

Changes in the temperature also cause a change in the peak positions of the Raman spectra. As temperature increases, there is a linear red shift in the 2D and G peaks due to increased anharmonic coupling of phonons and increased thermal expansion in the lattice, [52] such that Raman spectroscopy can be used to derive the temperature of graphene [53, 54]. The ability to use Raman as a thermometer opens up the possibility of using Raman to measure such quantities as thermal conductivity in a local, noninvasive way [55, 56].

5. STUDY OF GRAPHENE DISORDER THROUGH RAMAN SPECTROSCOPY

Now we will focus on the characterization of disorder in graphene caused by electron-beam irradiation and oxygen plasma exposure [57, 58]. The effect of electron-beam irradiation on graphene and graphene devices is of particular importance because of the prevalence of electron beams in both imaging of graphene, e.g. scanning electron microscopy (SEM) and transmission electron microscopy (TEM), and fabrication of graphene devices using electron-beam lithography (EBL). In addition, such studies are important to develop radiation-hard graphene-based electronics that can stand up to extreme conditions such as charged particle irradiation in space [59]. Many studies have used energetic electrons to study disorder in graphene [57, 60-64].

Plasma etching is also a common tool used to pattern graphene nanostructures, such as Hall bars [2] and nanoribbons [65]. In addition, plasma etching is used to study how graphene's properties are affected by etching-induced disorder [58, 66-70]. Other techniques that have been used to create artificial defects in graphene include ozone exposure [71], high-temperature oxidation [72] and energetic irradiation by positive ions [19, 73-78] and protons [79].

First, to study the effect of electron-beam irradiation [57], a graphene sample is placed in a scanning electron microscope (SEM), and a 25 μm by 25 μm area is continuously scanned by the electron beam. The beam’s kinetic energy is 30 keV,

and the beam current is 0.133 nA. The accumulated time exposed to the electron-beam (T_e) determines the accumulated irradiation dosage (D_e) (e.g. T_e = 60 s gives D_e = 100 e^-/nm^2). In comparison, the typical exposure used in a lithography process is around 1 e^-/nm^2. SEM imaging typically exposes samples to at least 100 e^-/nm^2.

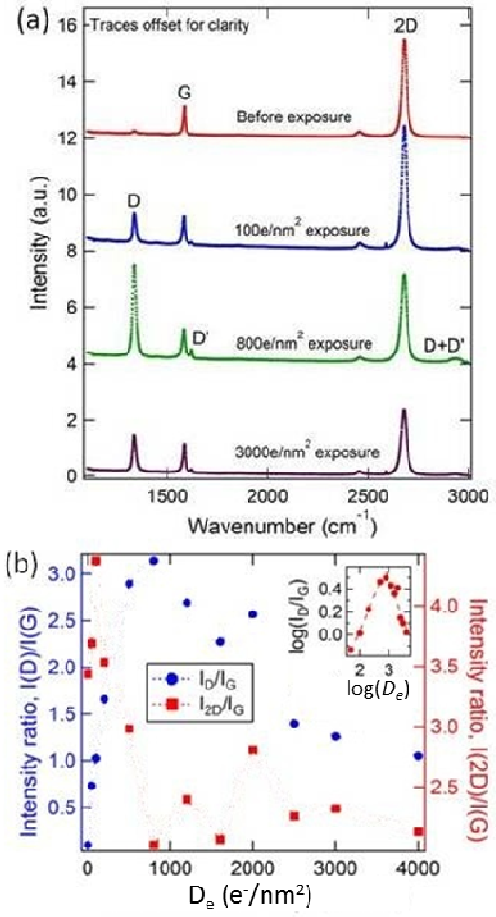

Figure 7. (Color online) (a) Raman spectra (excitation wavelength 532 nm) for a progression of accumulated electron-beam exposures on graphene sample "A." The spectra are offset vertically for clarity. (b) The full progression of the ratios of Raman peak intensities ID/IG and I2D/IG plotted against the accumulated dosage of energetic electrons (De). The inset of (b) shows the log of ID/IG plotted against the log of De. The dotted lines are linear fits for the low (left, slope = 0.6) and high (right, slope = -0.9) defect regimes.

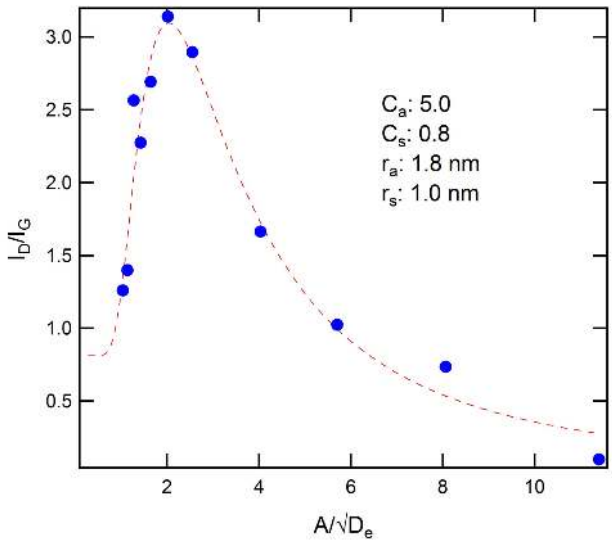

Figure 8. (Color online) I_D/I_G of electron-beam irradiated graphene plotted against $A/\sqrt{D_e}$, a quantity approximating L_D for A = 57. The dashed line is a fitting derived from Eq. (1), which fits well with the data.

After each successive exposure, the graphene device is removed from the scanning electron microscope, and room condition measurements are promptly performed with a 532 nm excitation laser.

Prior to exposure, the Raman spectrum of device "A" shows the signature for pristine single-layer graphene, with a G peak at ~1580 cm^{-1} and a 2D peak at ~2690 cm^{-1}, with a ratio of the intensities of the 2D and G peaks, I_{2D}/I_G, of 3.4.

Figure 7 shows how the Raman spectra evolve with increased electron-beam irradiation. Representative spectra are shown in Fig. 7(a), demonstrating the increase of the D peak, as well as the emergence of the D´ and D+G peaks. After higher exposures, these peaks attenuate.

This can be seen more clearly in Fig. 7(b), which shows the progression of the peak intensity ratios (I_D/I_G and I_{2D}/I_G) as functions of D_e. I_D/I_G behaves as expected, increasing in the low disorder regime (D_e < 800 e^-/nm^2) and decreasing in the high disorder regime (D_e > 800 e^-/nm^2). I_D/I_G begins at ~0 before the exposure and then increases with increasing D_e in the low-defect-density regime to ~3 after 800 e^-/nm^2, and I_D/I_G then decreases with further increasing D_e in the high-defect-density regime to ~1 for D_e = 4000 e^-/nm^2.

In our experiment, we assume the total electron beam dosage per unit area to be proportional to the defect concentration, $1/L_D^2$, therefore $L_D \propto 1/\sqrt{D_e}$. We can plot I_D/I_G with respect to $A/\sqrt{D_e}$, where A = 57 is a proportionality constant chosen such that the peak of the I_D/I_G curve appears at $A/\sqrt{D_e}$ = 2 nm [21]. We can add a fitting line based on Eq. (1) to calculate r_a (1.8 nm), r_s (1 nm), C_a (5) and C_s (0.8) seen in Fig. 8. We note that we find similar values as for the argon ion study by Lucchese *et al* [19].

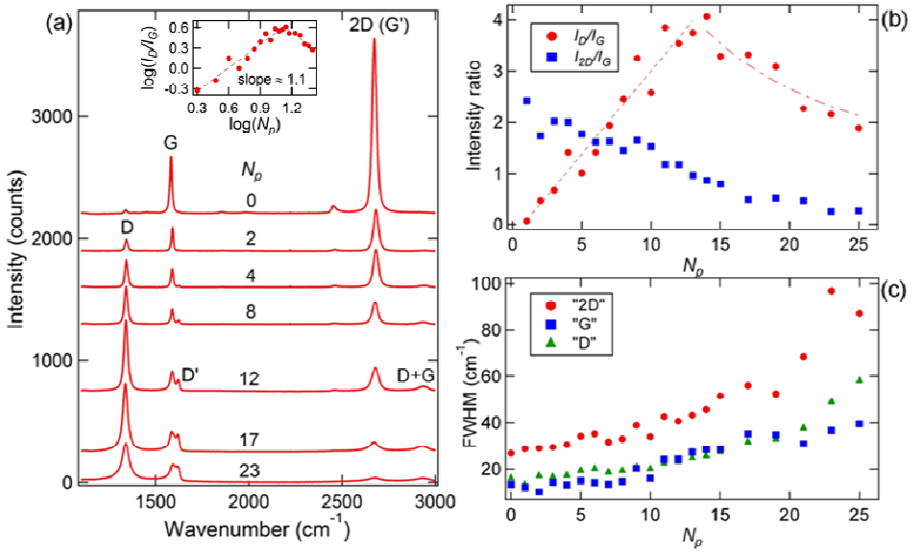

Figure 9. (Color online) (From [58]) (a) Raman spectra (excitation wavelength 532 nm) of single layer graphene sample "B" after various numbers of accumulated oxygen plasma pulses, N_p. The spectra are offset vertically for clarity. The inset shows log(I_D/I_G) plotted against log(N_p), with the dashed lines representing linear fits to the low-defect (left side, slope = 1.1) and high-defect (right side, slope = -1.2) regimes. (b) Ratios of Raman peak intensities, I_D/I_G and I_{2D}/I_G plotted against N_p. The dashed line is a fitting for $I_D/I_G = C/L_D^2$ (low-defect-density regime), and the dot-dashed line is a fitting for $I_D/I_G = D \cdot L_D^2$ (high-defect-density regime), where L_D is proportional to $N_p^{-0.5}$. The inset of (a) shows log(I_D/I_G) plotted against log(N_p). (c) The FWHM of the 2D, G and D peaks are plotted as functions of N_p.

We also studied the Raman spectra of graphene exposed to various amounts of oxygen plasma [58]. Our graphene samples are exposed cumulatively to short pulses (~ ½ seconds) of oxygen plasma in a microwave plasma system (Plasma-

Preen II-382) operating at 100 W. A constant flow of O_2 is pumped through the sample space, and the gas is excited by microwaves (manually pulsed on and off). The microwaves generate ionized oxygen plasma, which has an etching effect on graphene and thus creates defects in graphene. Raman measurements are performed in room conditions after each pulse.

Figure 9 shows the progression of the Raman spectrum as a function of the number (N_p) of plasma-etching pulses. The dependence of I_D/I_G on N_p shows 2 different behaviors in the low and high defect regimes, much like for electron-beam exposure. I_D/I_G begins at ~0 before the plasma exposure. I_D/I_G increases with increasing N_p to ~4 after 14 plasma exposures, and then decreases with further increasing N_p in the high-defect-density regime to ~1.9 for $N_p = 25$. On the other hand, the ratio of the intensities of the "2D" and "G" peaks, I_{2D}/I_G, continuously decreases with increasing N_p from ~3 for $N_p = 0$ down to ~ 0.3 for $N_p = 25$.

While we find the plasma etching data does not fit well to Eq. (1), they still can be fitted to Eqs. (2) and (4) if we assume the total exposure time to be proportional to the defect concentration, $1/L_D^2$ such that $L_D \propto 1/\sqrt{N_p}$. In Fig. 9(b), the data in the low-defect-density regime are fitted to

$$\frac{I_D}{I_G} = C \times N_p \quad \text{(dashed line)}, \tag{5}$$

and those in the high-defect-density regime are fitted to

$$\frac{I_D}{I_G} = \frac{C}{N_p} \quad \text{(dot-dashed line)}. \tag{6}$$

where Eq. (5) corresponds to Eq. (2) and Eq. (6) corresponds to Eq. (4).

The inset of Fig. 9(a) shows $\log(I_D/I_G)$ versus $\log(N_p)$. A line fit of the data in the low-defect-density regime gives a slope of ~1.1, confirming the approximate linear relationship between I_D/I_G and N_p in that regime, agreeing well with Eq. (2). A line fit in the high-defect-density regime gives a slope ~-1.2, again consistent with Eq. (6) or Eq. (4).

$C(\lambda)$ is given to be 102 nm^2 for λ = 514 nm [19]. Assuming comparable $C(\lambda)$ for our slightly different λ (532 nm), we estimate $L_D \approx 5$ nm at the peak of I_D/I_G (~4), a value similar to other reported values [19, 78].

The gradual decrease of the 2D peak is also consistent with previous work [66, 68, 72]. The decreasing I_{2D}/I_G versus N_p is likely mainly due to the defect-induced suppression of the lattice vibration mode corresponding to the 2D peak.

Figure 9(c) shows the FWHM of the 2D, G and D peaks as functions of N_p. The peaks widen with increasing N_p, especially at higher exposures. Defects in the crystal lattice decrease the phonon lifetime, which in turn widens the Raman peaks [80].

6. CONCLUSION

The applications of Raman spectroscopy to characterizing graphitic materials has become increasingly widespread. The sensitivity of the positions, widths and intensities of the D, G and 2D peaks has made it possible to probe a variety of attributes. The effects of edge states, strain, doping, temperature, thickness and disorder are all discernible in the Raman spectrum of graphene and other graphitic materials given the proper conditions. This has given us a powerful, noninvasive tool for graphene characterization.

REFERENCES

[1] Geim, A. K. and Novoselov, K. S. *Nature Mater.* 2007, 6, 183-191.

[2] Raza, H. *Graphene Nanoelectronics: Metrology, Synthesis, Properties and Applications*; Springer: Berlin, 2012.

[3] Berger, C.; Song, Z.; Li, X.; Wu, X.; Brown, N.; Naud, C.; Mayou, D.; Li, T.; Hass, J.; Marchenkov, A. N.; Conrad, E. H.; First, P. N.; de Heer, W. A. *Science* 2006, 312 1191-1196.

[4] Schwierz, F. *Nature Nanotech.* 2010, 5, 487-496.

[5] Schedin, F.; Geim, A. K.; Morozov, S. V.; Hill, E. W.; Blake, P.; Katsnelson, M. I.; Novoselov, K. S. *Nature Mater.* 2007, 6, 652-655.

[6] Bae, S.; Kim, H.; Lee, Y.; Xu, X. F.; Park, J. S.; Zheng, Y.; Balakrishnan, J.; Lei, T.; Kim, H. R.; Song, Y. I.; Kim, Y. J.; Kim, K. S.; Ozyilmaz, B.; Ahn, J. H.; Hong, B. H.; Iijçima, S. *Nature Nanotech.* 2010, 5, 574-578.

[7] Gardiner, D. J. *Practical Raman Spectroscopy*; Springer-Verlag: Berlin, 1989.

[8] Saito, R.; Hofmann, M.; Dresselhaus, G.; Jorio, A.; Dresselhaus, M. S. *Adv. Phys.* 2011, 30, 413-550.

[9] Ferrari, A. C. *Solid State Commun.* 2007, 143, 47-57.
[10] Ferrari, A. C.; Meyer, J. C.; Scardaci, V.; Casiraghi, C.; Lazzeri, M.; Mauri, F.; Piscanec, S.; Jiang, D.; Novoselov, K. S.; Roth, S.; Geim, A. K. *Phys. Rev. Lett.* 2006, 97, 187401.
[11] Gupta, A.; Chen, G.; Joshi, P.; Tadigadapa, S.; Eklund, P. C. *Nano. Lett.* 2006, 6, 2667-2673.
[12] Lespade, P. and Marchand, A. *Carbon* 1984, 22, 375-385.
[13] Ni, Z. H.; Wang, Y. Y.; Yu, T.; You, Y.; Shen, Z. X. *Phys. Rev. B* 2008, 77, 235403.
[14] Tuinstra, F. and Koenig, L. *J. Chem. Phys.* 1970, 53, 1126-1130.
[15] Thomsen, C. and Reich, S. *Phys. Rev. Lett.* 2000, 85, 5214-5217.
[16] Narula, R. and Reich, S. *Phys. Rev. B* 2008, 78, 165422.
[17] Venezuela, P.; Lazzeri, M.; Mauri, F. *Phys. Rev. B* 2011, 84, 035433.
[18] Saito, R.; Jorio, A.; Souza Filho, A. G.; Dresselhaus, G.; Dresselhaus, M. S.; Pimenta, M. A. *Phys. Rev. Lett.* 2002, 88, 027401.
[19] Lucchese, M. M.; Stavale, F.; Ferreira, E. H.; Vilani, C.; Moutinho, M. V. O.; Capaz, R. B.; Achete, C. A.; Jorio, A. *Carbon* 2010, 48, 1592-1597.
[20] Ferrari, A. C. and Robertson, J. *Phys. Rev. B* 2001, 64, 075414.
[21] Ferrari, A. C. and Robinson, J. *Phys. Rev. B* 2000, 61, 14095-14107.
[22] Martins Ferreira, E. H.; Moutinho, M. V. O.; Stavale, F.; Lucchese, M. M.; Capaz, R. B.; Achete, C. A.; Jorio, A. Phys Rev. B 2010, 82, 125429.
[23] Cançado, L. G.; Jorio, A.; Martins Ferreira, E. H.; Stavale, F.; Achete, C. A.; Capaz, R. B.; Moutinho, M. V. O.; Lombardo, A.; Kulmala, T. S.; Ferrari, A. C. *Nano Lett.* 2011, 11, 3190-3196.
[24] Cançado, L. G.; Takai, K.; Enoki, T.; Endo, M.; Kim, Y. A.; Mizusaki, H.; Jorio, A.; Coelho, L. N.; Magalhães-Paniago, R.; Pimenta, M. A. *Appl. Phys. Lett.* 2006, 88, 163106.
[25] Novoselov, K. S.; Jiang, D.; Schedin, F.; Booth, T. J.; Khotkevich, V. V.; Morozov, S. V.; Geim, A. K. *Proc. Natl. Acad. Sci. USA* 2005, 102, 10451-10453.
[26] Yu, Q. K.; Lian, J.; Siripongert, S.; Li, H.; Chen, Y. P.; Pei, S. S. *Appl. Phys. Lett.* 2008, 93, 113103.
[27] Reina, A.; Jia, X.; Ho, J.;Nezich, D.; Son, H.; Bulovic, V.; Dresselhaus, M. S.; Kong, J. *Nano Lett.* 2009, 9, 30-35.
[28] Kim, K. S.; Zhao, Y.; Jang, H.; Lee, S. Y.; Kim, J. M.; Kim, K. S.; Ahn, J.-H.; Kim, P.; Choi, J.-Y.; Hong, B. H. *Nature* 2009, 457, 706-710.
[29] Cao, H.; Yu, Q.; Colby, R.; Pandey, D.; Park, C. S.; Lian, J.; Zemlyanov, D.; Childres, I.; Drachev, V. Stach, E. A.; Hussain, M.; Li, H.; Pei, S. S.; Chen, Y. P. *J. Appl. Phys.* 2010, 107, 044310.

[30] Li, X.; Cai, W.; An, J.; Kim, S.; Nah, J.; Yang, D.; Piner, R.; Velamakanni, A.; Jung, I.; Tutuc, E.; Banerjee, S. K.; Colombo, L.; Ruoff, R. S. *Science* 2009, 324, 1312-1314.

[31] Cao, H.; Yu, Q.; Jauregui, L. A.; Tian, J.; Wu, W.; Liu, Z.; Jalilian, R.; Benjamin, D. K.; Jiang, Z.; Bao, J.; Pei, S. S.; Chen, Y. P. *Appl. Phys. Lett.* 2010, 96, 122106.

[32] Stankovich, S.; Dikin, D. A.; Dommett, G.; Kohlhaas, K. A.; Zimney, E. J.; Stach, E. A.; Piner, R. D.; Nguyen, S. T.; Ruoff R. S. *Nature* 2006, 442, 282-286.

[33] Stankovich, S.; Dikin, D. A.; Piner, R. D.; Kohlhaas, K. A.; Kleinhammes, A.; Jia, Y.; Wu, Y.; Nguyen, S. T.; Ruoff R. S. *Carbon* 2007, 45, 1558-1565.

[34] Park, S.; Dikin, D. A.; Nguyen, S. T.; Ruoff, R. S. *J. Phys. Chem. C* 2009, 113, 15801-15804.

[35] Casiraghi, C.; Hartschuh, A.; Qian, H.; Piscanec, S.; Georgi, C.; Fasoli, A.; Novoselov, K. S.; Basko, D. M.; Ferrari, A. C. *Nano Lett.* 2009, 9, 1433-1441.

[36] Graf, D.; Molitor, F.; Ensslin, K.; Stampfer, C.; Jungen, A.; Hierold, C.; Wirtz, L. *Nano Lett.* 2007, 7, 238-242.

[37] Cançado, L. G.; Pimenta, M. A.; Neves, B. R. A.; Dantas, M. S. S.; Jorio, A. *Phys. Rev. Lett.* 2004, 93, 247401.

[38] Cançado, L. G.; Jorio, A.; Pimenta, M. A. *Phys. Rev. B* 2007, 76, 064304-064310.

[39] You, Y.; Ni, Z. H.; Shen, Z. X. *Appl. Phys. Lett.* 2008, 93, 163112.

[40] Sasaki, K.; Saito, R.; Wakabayashi, K.; Enoki, T. *J. Phys. Soc. Jpn.* 2010, 79, 044603.

[41] Cong, C.; Yu, T.; Wang, H. *ASC Nano* 2010, 4, 3175-3180.

[42] Saito, R.; Furukawa, M.; Dresselhaus, G.; Dresselhaus, M. S. *J. Phys.: Condens. Matter* 2010, 22, 334203

[43] Yu, Q.; Jauregui, L. A.; Wu, W.; Colby, R.; Tian, J.; Su, Z.; Cao, H.; Liu, Z.; Pandey, D.; Wei, D.; Chung, T. F.; Peng, P.; Guisinger, N. P.; Stach, E. A.; Bao, J.; Pei, S.; Chen, Y. P. *Nature Mater.* 2011, 10, 443-449.

[44] Pisana, S.; Lazzeri, M.; Casiraghi, C.; Novoselov, K. S.; Geim, A. K.; Ferrari, A. C.; Mauri, F. *Nature Mater.* 2007, 6, 198-201.

[45] Das, A.; Pisana, S.; Chakraborty, B.; Piscanec, S.; Saha, S. K.; Waghmare, U. V.; Novoselov, K. S.; Krishnamurthy, H. R.; Geim, A. K.; Ferrari, A. C.; Sood, A. K. *Nature Nano.* 2008, 3, 210-215.

[46] Mohiuddin, G.; Lombardo, A.; Nair, R. R.; Bonetti, A.; Savini, G.; Jalil, R.; Bonini, N.; Basko, D. M.; Galiotis, C.; Marzari, N.; Novoselov, K. S.; Geim, A. K.; Ferrari, A. C. *Phys. Rev. B* 2009, 79, 205433.
[47] Ni, Z. H.; Yu, T.; Lu, Y. H.; Wang, Y. Y.; Feng, Y. P.; Shen, Z. X. *ACS Nano* 2008, 2, 2301-2305.
[48] Yu, T.; Ni, Z. H.; Du, C. L.; You, Y. M.; Wang, Y. Y.; Shen, Z. X. *J. Phys. Chem. C* 2008, 112, 12602-12605.
[49] Huang, M.; Yan, H.; Chen, C.; Song, D.; Heinz, T. F.; Hone, J. *Proc. Nat. Acad. Sci. USA* 2009, 106, 7304-7308.
[50] Tsoukleri, G.; Partenios, J.; Papagelis, K.; Jalil, R.; Ferrari, A. C.; Geim, A. K.; Novoselov, K. S.; Galiotis, C. *Small* 2009, 5, 2397-2402.
[51] Frank, O.; Tsoukleri, G.; Parthenios, J.; Papagelis, K.; Riaz, I.; Jalil, R.; Novoselov, K. S.; Galiotis, C. *ASC Nano* 2010, 4, 3131-3138.
[52] Postmus, C.; Ferraro, J. R.; Mitra, S. S. *Phys. Rev.* 1968, 174, 983-987.
[53] Calizo, I.; Miao, F.; Bao, W.; Lau, C. N.; Balandin, A. A. *Appl. Phys. Lett.* 2007, 91, 071913.
[54] Calizo, I.; Balandin, A. A.; Bao, W.; Miao, F.; Lau, C. N. *Nano Lett.* 2007, 7, 2645-2649.
[55] Balandin, A. A.; Ghosh, S.; Bao, W.; Calizo, I.; Teweldebrhan, D.; Miao, F.; Lau, C. N. Nano Lett. 2008, 8, 902-907.
[56] Jauregui, L. A.; Yue, Y.; Sidorov, A. N.; Hu, J.; Yu, Q.; Lopez, G.; Jalilian, R.; Benjamin, D. K.; Delk, D. A.; Wu, W.; Liu, Z.; Wang, X.; Jiang, Z.; Ruan, X.; Bao, J.; Pei, S. S.; Chen, Y. P. *ECS Trans.* 2010, 28(5), 73
[57] Childres, I.; Jauregui, L. A.; Foxe, M.; Tian, J.; Jalilian, R.; Jovanovic, I.; Chen, Y. P. *Appl. Phys. Lett.* 2010, 97, 173109.
[58] Childres, I.; Jauregui, L. A.; Tian, J.; Chen, Y. P. *New J. Phys.* 2011, 13, 025008.
[59] Claeys, C. and Simoen, E. *Radiation Effects in Advanced Semiconductor Materials and Devices*; Springer: Berlin, 2002.
[60] Teweldebrhan, D. and Balandin, A. A. *Appl. Phys. Lett.* 2009, 94, 013101.
[61] Teweldebrhan, D. and Balandin, A. A. *Appl. Phys. Lett.* 2009, 95, 246101.
[62] Liu, G.; Teweldebrhan, D.; Balandin, A. A. *IEEE Trans. Nanotech.* 2010, 10, 865-870.
[63] Rao, G.; Mctaggart, S.; Lee, J. L.; Geer, G. E. *Mater. Res. Soc. Symp. Proc.* 2009, 1184, HH03-07.
[64] Xu, M.; Fujita, D.; Hanagata, N. *Nanotechnology* 2010, 21, 265705.
[65] Han, M. Y.; Ozyilmaz, B.; Zhang, Y. B.; Kim, P. *Phys. Rev. Lett.* 2007, 98, 206805.

[66] Kim, D. C.; Jeon, D.; Chung, H.; Woo, Y. S.; Shin, J. K.; Seo, S. *Nanotechnology* 2009, 20, 375703.
[67] Kim, K.; Park, H. J.; Woo, B.; Kim, K. J.; Kim, G. T.; Yun, W. S. *Nano Lett.* 2008, 8, 3092-3096.
[68] Shin, Y. J.; Wang, Y. Y.; Huang, H.; Kalon, G.; Thye, A.; Wee, S.; Shen, Z.; Bhatia, C. S.; Yang, H. *Langmuir* 2010, 26, 3798-3802.
[69] Gokus, T.; Nair, R. R.; Bonetti, A.; Boehmler, M.; Lombardo, A.; Novoselov, K. S.; Geim, A. K.; Ferrari, A. C.; Hartschuh, A. *ASC Nano* 2009, 3, 3963-3968.
[70] Kim, K.; Choi, J.; Lee, H.; Jung, M. C.; Shin, H. J.; Kang, T.; Kim, B.; Kim, S. *J. Phys. Condens. Matter* 2010, 22, 045005.
[71] Moser, J.; Tao, H.; Roche, S.; Alzina, F.; Torres, C. M. S.; Bachtold, A. *Phys. Rev. B* 2010, 81, 205445.
[72] Liu, L.; Ryu, S.; Yomasik, M. R.; Stolyarova, E.; Jung, N.; Hybertsen, M. S.; Steigerwald, M. L.; Brus, L. E.; Flynn, G. W. *Nano Lett.* 2008, 8, 1965-1970.
[73] Giannazzo, F.; Sonde, S.; Raineri, V.; Rimini, E. *Appl. Phys. Lett.* 2009, 95, 263109.
[74] Compagnini, G.; Giannazzo, F.; Sonde S.; Raineri, V.; Rimini, E. *Carbon* 2009, 47, 3201-3207.
[75] Tapaszto, L.; Dobrik, G.; Nemes-Incze, P.; Vertesy, G.; Lambii, P.; Biro, L. P. *Phys. Rev. B* 2008, 78, 233407.
[76] Chen, J.; Cullen, W. G.; Jang, C.; Fuhrer, M. S.; William, E. D. *Phys. Rev. Lett.* 2009, 102, 236805.
[77] Lopez, J. J.; Greer, F.; Greer, J. R. *J. Appl. Phys.* 2010, 107, 104326.
[78] Tan, C. L.; Tan, Z. B.; Ma, L.; Qu, F. M.; Yang, F.; Chen, J.; Liu, G. T.; Yang, H. F.; Yang, C. L.; Lu, L. *Sci. China Ser. G – Phys. Mech. Astron.* 2009, 52, 1293-1298.
[79] Arndt, A.; Spoddig, D.; Esquinazi, P.; Barzola-Quiquia, J.; Durari, S.; Butz, T. *Phys. Rev. B* 2009, 80, 195402.
[80] Di Bartolo, B. *Optical Interactions in Solids*; Wiley: New York, 1968.